Journal of Nuclear Materials 377 (2008) 232–242

Contents lists available at ScienceDirect

Journal of Nuclear Materials

journal homepage: www.elsevier.com/locate/jnucmat

Corrosion rate of parent and weld materials of F82H and JPCA steels under LBE flow with active oxygen control at 450 and 500 °C

Kenji Kikuchi [a,*], Kinya Kamata [b], Mikinori Ono [b], Teruaki Kitano [b], Kenichi Hayashi [b], Hiroyuki Oigawa [a]

[a] Japan Atomic Energy Agency, Tokai-mura, Naka-gun, Ibaraki-ken 319-1195, Japan
[b] Mitsui Engineering and Ship-building Co., Ltd., 5-6-4 Tsukiji, Chuo-ku, Tokyo 104-8439, Japan

A B S T R A C T

Corrosion behavior of parent and weld materials of F82H and JPCA was studied in the circulating LBE loop under impinging flow. These are candidate materials for Japanese Accelerator Driven System (ADS) beam windows. Maximum temperatures were kept to 450 and 500 °C with 100 °C constant temperature difference. Main flow velocity was 0.4–0.6 m/s in every case. Oxygen concentration was controlled to $2–4 \times 10^{-5}$ mass% although there was one exception. Testing time durations were 500–3000 h. Round bar type specimens were put in the circular tube of the loop. An electron beam weld in the middle of specimens was also studied. Optical microscopy, electron microscopy, X-ray element analyses and X-ray diffraction were used to investigate corrosion in these materials. Consequently corrosion depth and stability of those oxide layers were characterized based on the analyses. For a long-term behavior a linear law is recommended to predict corrosion in the ADS target design.

1. Introduction

Lead bismuth eutectic (LBE) is to be used as a spallation target and reactor coolant in an accelerator driven nuclear transmutation system (ADS). In order to realize ADS, one of the main issues is to determine corrosion properties of materials under flowing LBE. In the Japanese ADS design proposed by Japan Atomic Energy Agency (JAEA) [1], candidate materials to be utilized for a beam window are ferritic–martensitic steel, F82H, and austenitic stainless steel, JPCA [2,3]. Hitherto, investigations of materials corrosion under flowing LBE condition were done by using martensitic steels and austenitic stainless steels [14–18]. The corrosion tests were carried in the parallel flow condition where specimens were set up in the flowing channel parallel to the LBE flow. So far modified F82H, which replaces elements producing long-lived isotopes such as Mo and Nb by W, was investigated in the loop but oxygen concentration in the melt eutectic was not measured [16]. F82H was investigated at higher temperature, 550 °C, under active oxygen control but at lower oxygen concentration of 2×10^{-9} wt% and under parallel flow condition [18]. However, the proton beam window is to be submerged in the reactor vessel under impinging LBE flow condition in the ADS design. The position is thought to be the most severe part where incident proton penetrates the plate under LBE flow cooling [4]. Thus studies are needed on JPCA corrosion in the flowing LBE. We have done corrosion tests of candidate materials, F82H and JPCA, under impinging flow condition at temperatures of 450 and 500 °C. Temperature difference in the corrosion test loop was decided to be 100 °C in every case with a reference design of 800 MWth power design. The objective of this study is to evaluate corrosion rate of not only the parent materials but also electron beam welded materials applicable to join a thin plate without distortions due to excess heat.

2. Experiment

2.1. Test loop

The LBE loop at MES, Mitsui Engineering & Ship-building Co., Ltd., was used for corrosion tests, which consists of test section, heater, economizer, electro-magnetic flow meter, electro-magnetic pump, filter, expansion tank, cooler, circulating pipe and dump tank as shown in Fig. 1 [5]. Oxygen concentration was controlled by adding hydrogen and/or moisture with argon carrier gas, and monitored by Bi/Bi_2O_3 type oxygen sensor.

2.2. Materials

Materials tested are ferritic–martensitic steel F82H [2], austenitic stainless steel JPCA [3] and the electron beam welding of those materials. Chemical compositions of the materials are listed in Table 1. Welded materials are prepared from bead-on-plate with 15 mm in depth of melting. F82H steel was welded after pre-heating at 300 °C, heat-treated at 300 °C in 2 h, and then annealed at 750 °C for 2 h for stress relieving. No heat-treatment was done after welding the JPCA material.

* Corresponding author. Tel.: +81 29 282 5058; fax: +81 29 282 6489.
E-mail address: kikuchi.kenji21@jaea.go.jp (K. Kikuchi).

0022-3115/$ - see front matter © 2008 Elsevier B.V. All rights reserved.
doi:10.1016/j.jnucmat.2008.02.047

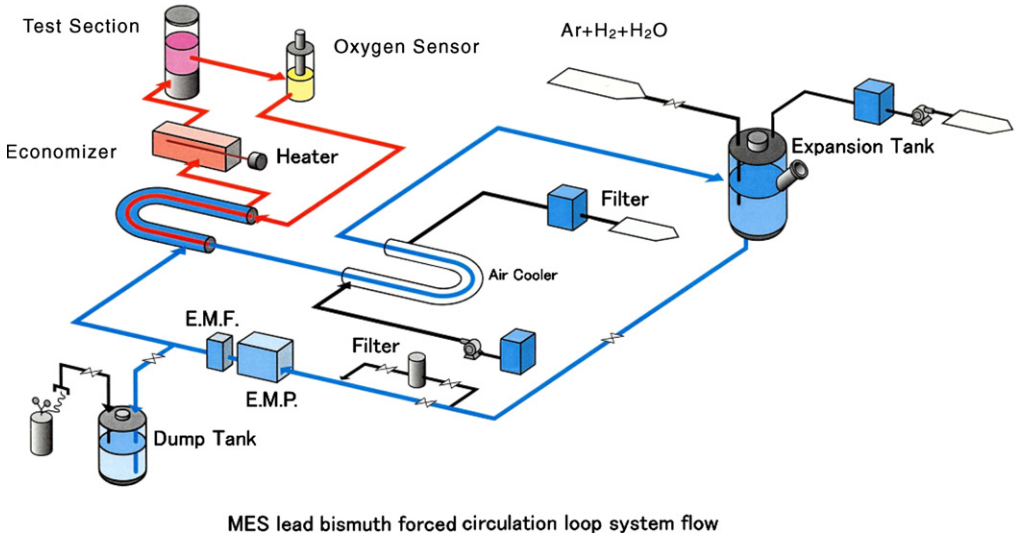

Fig. 1. Flow diagram of MES loop.

Table 1
Chemical compositions of F82H and JPCA (wt%)

	Cr	Ni	Mo	Ti	W	V	Ta	C	Fe
F82H	8	–	–	–	2	0.2	0.04	0.1	Bal
JPCA	15	15	2	0.25	–	–	–	0.06	Bal

Table 2
Test conditions

	Temperature (°C)	Time (h)
Case-1	450	1000
Case-2	450	3000
Case-3	500	1000

2.3. Specimen preparation

Specimen is a bar shape at a size of 8 mm in diameter and 130 mm in length. Surface preparation was done by buffing finally after mechanical shaping. Maximum surface roughness was 1.6 μm in F82H and 1 μm in JPCA, respectively, in the measurement of laser microscope. One end of specimen bar has a hemispherical shape setup in the upstream and other end was fixed to test holder in the downstream. The test holder includes two parallel flow channels with a round cross section of 12 mm in diameter. Specimens were setup in the channel. LBE flows in the main channel, impinges on the hemispherical edge of specimens and then passes through an annular flow channels. LBE velocity of the main duct is 0.5 m/s and 0.9 m/s in the annular channels, respectively, as shown in Fig. 2.

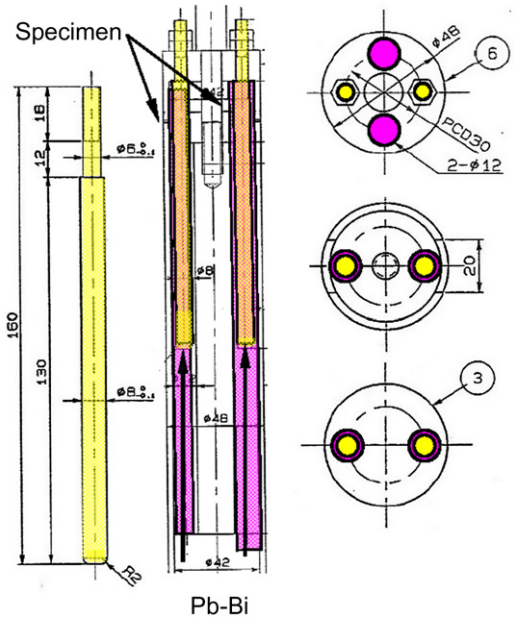

Fig. 2. Specimen in the test holder. The left figure is a detailed sketch of a specimen.

2.4. Test conditions

The conditions of corrosion tests are listed in Table 2. The described temperature means the scheduled values at the specimen position and time means the test duration. LBE velocity in the main channel is 0.5 m/s. Oxygen concentration is controlled to $2–4 \times 10^{-5}$ mass% by adding hydrogen and/or moisture with argon career gas, and monitored by Bi/Bi_2O_3 type oxygen sensor. Our study was done under known condition. Saturated oxygen concentration, C_s, in LBE is described by the next equation [19]:

$$\text{Log } C_s = 1.2 - 3400/T, \quad (1)$$

where T is absolute temperature in K. In the experiment C/C_s is about 0.2, where C is the oxygen concentration in LBE. This is a regime where iron oxide can be formed in LBE. The temperature difference between hot and cold region is 100 °C due to the ADS design [4].

3. Results

3.1. Optical microscopy

Fig. 3 shows micro and macro structures of specimens for F82H. Figs. 3(a) and (b) show the cross section at the middle part and the edge part of specimen, respectively. It is found that there was a welded zone with 1 mm in width accompanied by heat affected zone at the middle of the specimen. LBE collides with the round tip in the flow channel. Figs. 3(c) and (d) show the micro structure at welded part and tip region, respectively, after tests in Case-1

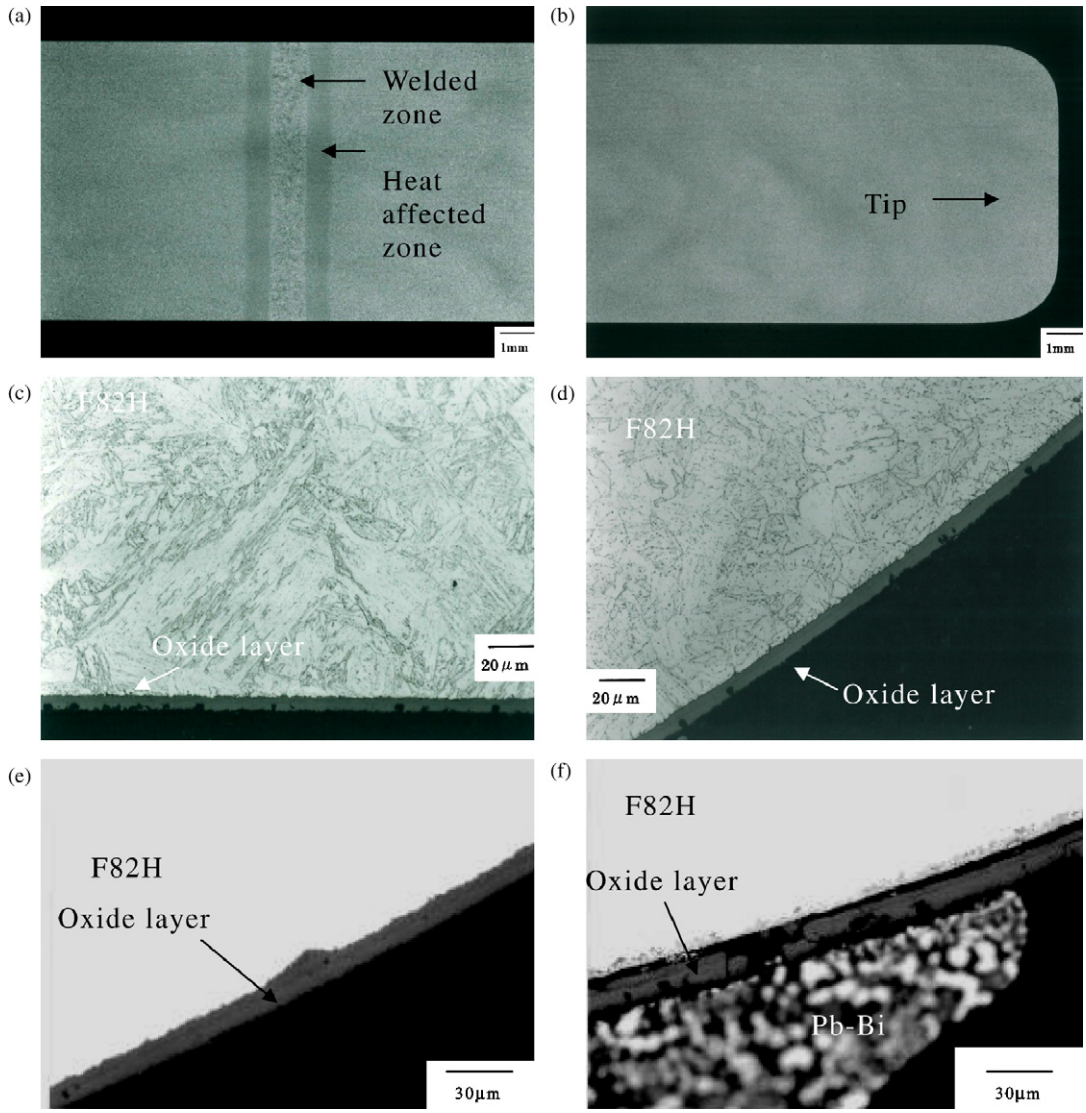

Fig. 3. Optical microscope observation of cross section for F82H specimens. (a) Macro structure including welded zone and heat affected zone, (b) macro structure including tip region at the right hand side where Pb–Bi impinges, (c) micro structure of welded zone tested at 450 °C for 1000 h, (d) micro structure of tip region tested at 450 °C for 1000 h, (e) cross section of tip region tested at 450 °C for 3000 h, and (f) cross section of tip region tested at 500 °C for 1000 h.

under the condition of 450 °C and 1000 h. It is found that the welded metal of F82H revealed coarse martensitic structure as compared to the fine microstructure in the non-welded tip region because of melting and re-solidification in weld process. Corrosion depth in F82H was limited near the surface of material. A failure of the corrosion layer could be observed but no crack was observed. Heat affected zone showed that martensitic structure became fine because of rapid heating and cooling during the weld process. Regardless of the difference in microstructures, corrosion layer showed no difference. Figs. 3(e) and (f) show the cross section of tip region tested at 450 °C for 3000 h and at 500 °C for 1000 h, respectively. In comparison with the results shown in Fig. 3(d) it is found that a corrosion depth increased with increasing test time duration at 450 °C, and with increasing test temperature. The corrosion layer was disintegrated at 500 °C.

Fig. 4 shows micro and macro structures of specimens for JPCA. Figs. 4(a) and (b) show the cross section at the middle part and the tip region of specimen, respectively. It is found that there is a welded zone with 1 mm in width but a heat affected zone was not visible, as compared to the case of F82H weldment. Figs. 4(c) and (d) show the micro structure at the welded part and tip region, respectively, after tests under the condition of 450 °C and 1000 h. It is found that the welded metal of JPCA exhibited dendritic structure. The corrosion layer was not visible by optical microscopy. Also no crack was observed. Fig. 4(e) shows the micro structure of specimens at the tip region, exposed for a longer time than the case in Fig. 4(d). It is characterized by shallow depression. Fig. 4(f) shows clear pits but no corrosion layer as was seen in F82H.

3.2. Scanning electron microscopy

Fig. 5 shows the cross section of parent material and of the welded region for F82H. Parent material showed a corrosion layer 6–8 μm in depth under the condition of 450 °C and 1000 h. The layer consists of two structures. An inner layer and/or an outer layer were failed. The thickness of the corrosion layer became 15 μm in depth at 3000 h. However, a failure of the corrosion layer was not seen for specimen tested for a longer duration.

Under the condition of 500 °C and 1000 h the corrosion layer grew to 15 μm in depth. A distinct structure that was clear at lower temperature was not seen by SEM but an additional layer was

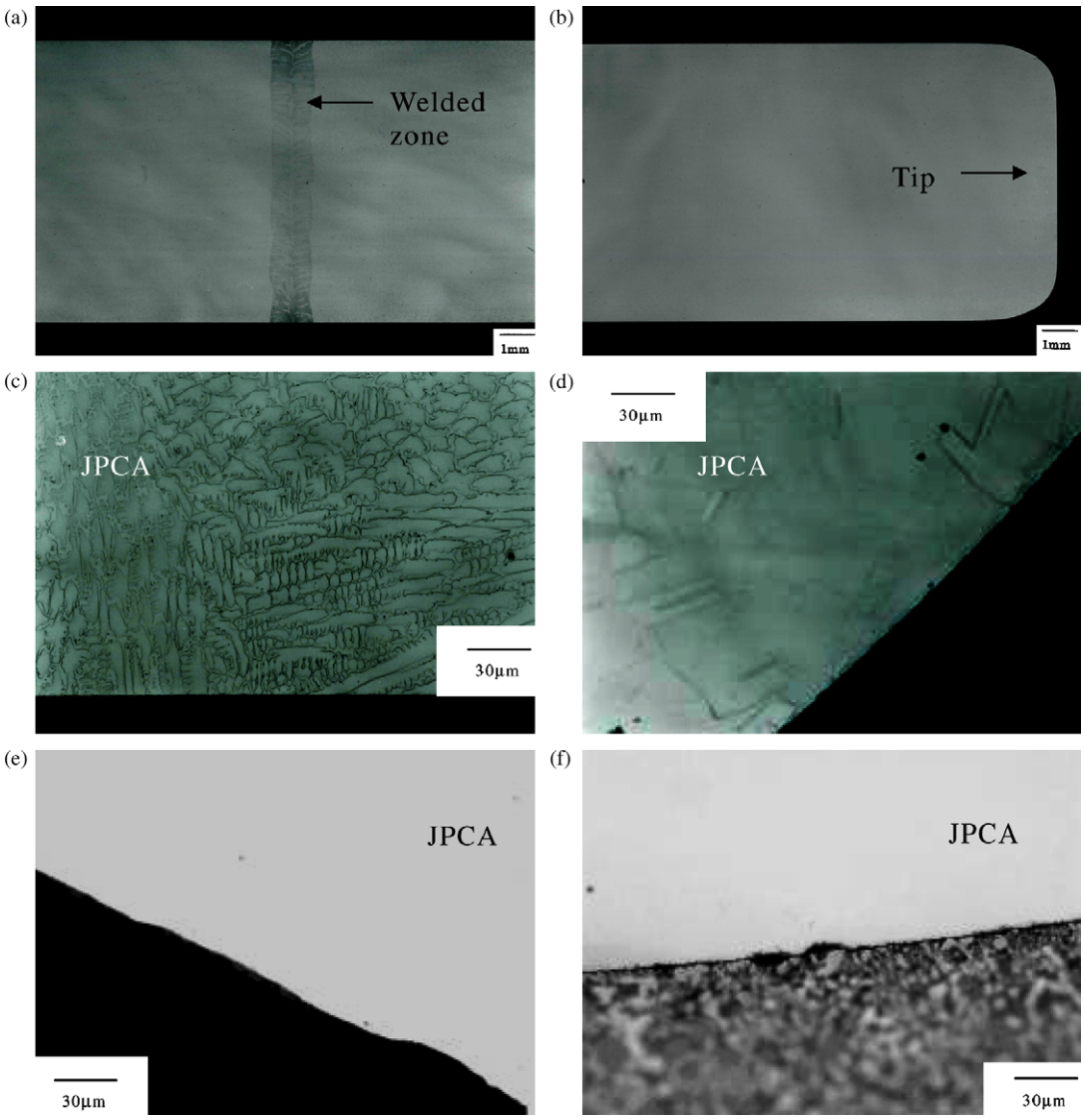

Fig. 4. Optical microscope observation of cross section for JPCA specimens. (a) Macro structure including welded zone, (b) macro structure including tip region at the right hand side where Pb–Bi impinges, (c) micro structure of welded zone tested at 450 °C for 1000 h, (d) micro structure of tip region tested at 450 °C for 1000 h, (e) cross section of tip region tested at 450 °C for 3000 h, and (f) cross section of tip region tested at 500 °C for 1000 h.

formed in the matrix, which could be observed in optical microscopy. Cracks penetrating these layers were extended parallel to the specimen surface. For the weld joint, a depth of corrosion layer as well as corrosion morphology showed the same results as with the parent material, except for that the two-layer structure was not seen for the specimens tested at 450 °C and 1000 h.

Fig. 6 shows the cross section of parent material and of the welded region for JPCA. As was seen in the optical microscopy a corrosion layer was not observed by SEM for the specimens tested at 450 °C and 1000 h. But at 3000 h a thin corrosion layer could be observed at 1–2 μm in depth. For the weld joint, a depth of corrosion layer as well as corrosion morphology showed the same results as with the parent material.

Fig. 7 showed pit growth observed in JPCA tested at 450 °C. A longer time test formed wide pits but not deep ones.

3.3. EPMA analyses

Fig. 8 showed elemental mapping of the cross section of the corrosion layer in the F82H parent material tested under the condition of 500 °C and 1000 h. In the SEM image two dark lines exists in parallel with specimen surface; the bottom line is located between matrix and corrosion layer and the upper line is the boundary between adhered lead-bismuth and corrosion layer. It is found by Fe image that corrosion layer consists of three layers. In comparison with Cr and Oxygen images the outer layer near lead-bismuth does not include Cr, and Fe as a main element there. In the middle layer Fe exists together with Cr and oxygen. The inner layer is 5 μm in thickness where diffused oxygen is recognized. Element mapping of Fe, Cr and oxygen at the welded part, heat affected zone and tip region showed the same as observed with the above result. As mentioned in Fig. 5 a diffusion layer of oxygen into the matrix was not seen at 450 °C.

Fig. 9 shows elemental mapping of the cross section of a corrosion layer in JPCA parent material tested under the condition of 500 °C and 1000 h.

Lead–bismuth is distinguished from JPCA by a dark line in SEM image. It is found that the corrosion layer of about 10 μm in thickness consists of two layers by comparing the reflected electron image (REI) and the Fe image. Fe and oxygen are main elements in the

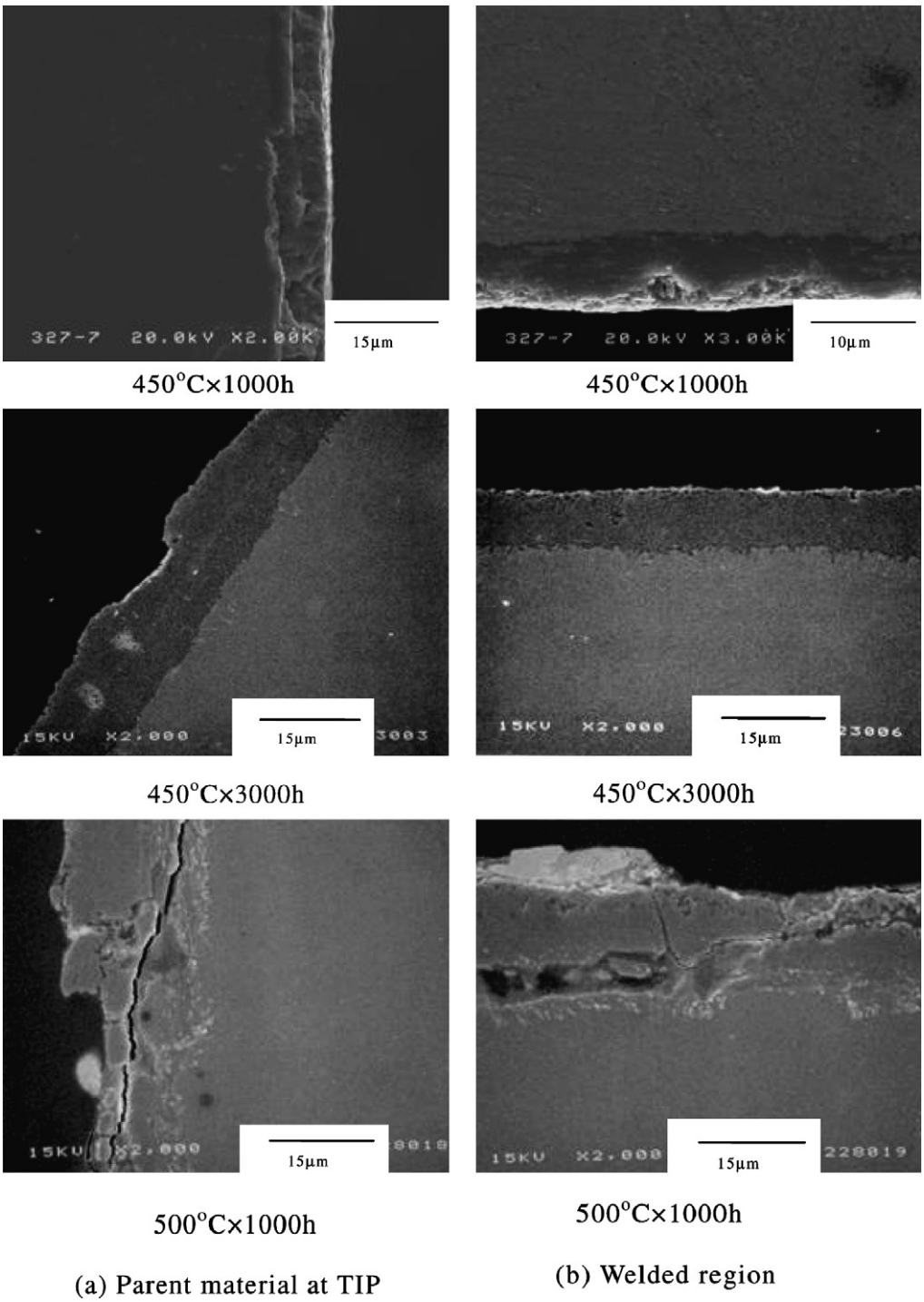

Fig. 5. SEM observation of F82H parent material and welded region.

outer layer and Cr and Ni as well as Fe and oxygen are also detected in the inner layer.

3.4. X-ray diffraction

Fig. 10 shows the results of X-ray diffraction analyses for F82H specimens under the condition of 1000 h at 450 °C, 1000 h at 500 °C and 3000 h at 450 °C. Peaks in diffraction angle coincide with M_3O_4, which indicates Fe_3O_4 or $FeCr_2O_4$.

Fig. 11 shows the results of X-ray diffraction analyses for JPCA specimens under the condition of 1000 h at 450 °C, 1000 h at 500 °C and 3000 h at 450 °C. Peaks in diffraction angle coincide with $Cr_{19}Fe_{70}Ni_{11}$ or FeNi at 450 °C, which corresponds with austenitic stainless steel. In addition with those peaks new ones are revealed at 500 °C, which is M_3O_4 type iron oxide.

3.5. Corrosion depth

Fig. 12 shows corrosion depth in F82H as a function of time. The corrosion depth is defined by the sum of thickness of both oxide layer and the oxygen diffusion depth but ignoring a possible loss of oxide layer. The corrosion depth was not always uniform so that

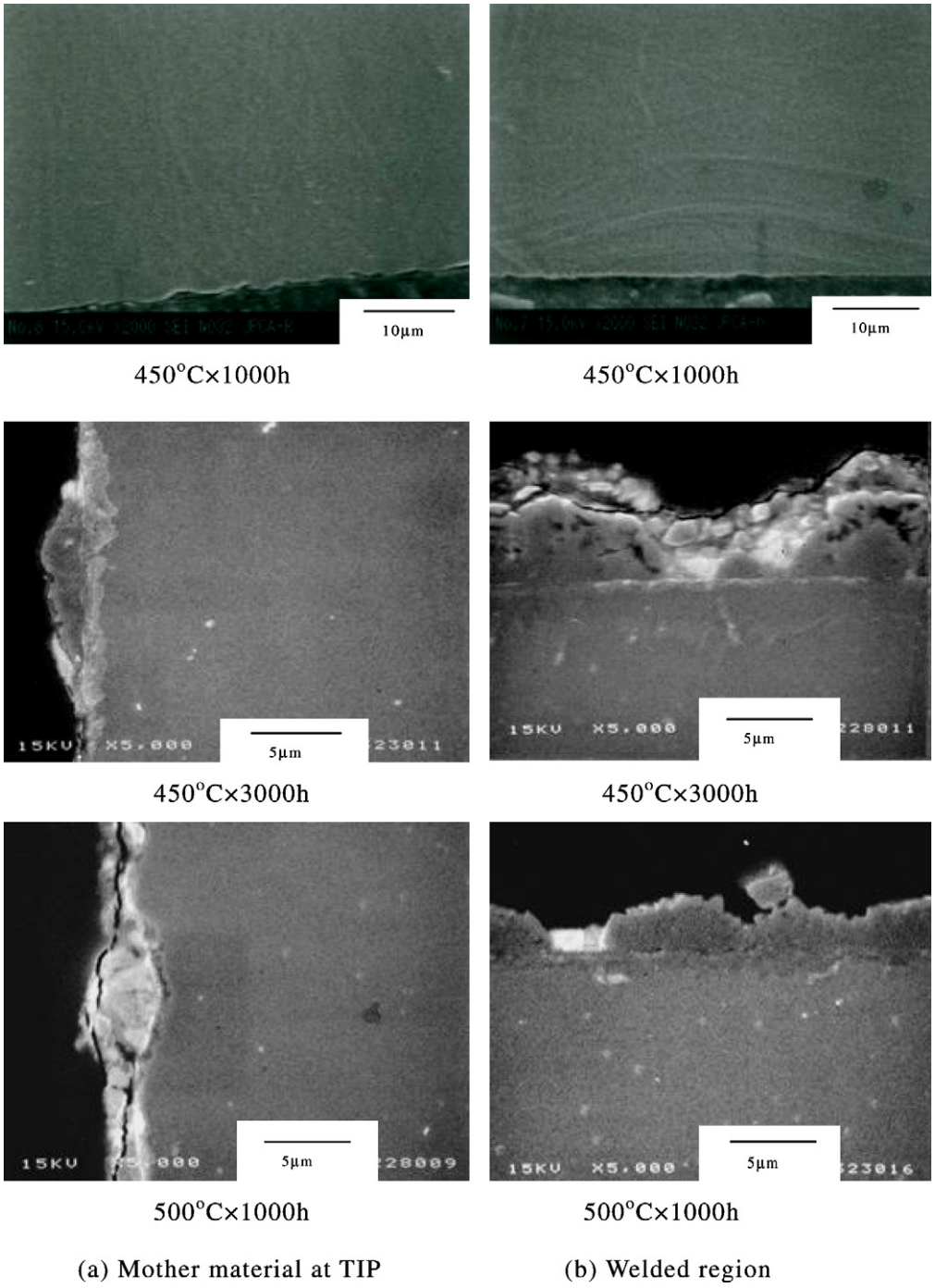

Fig. 6. SEM observation of JPCA parent material and welded region.

the maximum depth was also plotted in the figure. Corrosion rate was formulated by the next equation at 450 °C:

$$D = (Kt)^{0.5}, \tag{2}$$

D is corrosion depth (μm), t is time (h) and K is a coefficient. For the case of maximum depth $K^{0.5} = 0.31\ \mu m\ h^{-1}$ and $K^{0.5} = 0.21\ \mu m\ h^{-1}$ for the averaged value.

Fig. 13 shows corrosion depth in JPCA as a function of time. The corrosion depth is defined by the sum of thickness of both oxide layer and pit depth as shown in Fig. 7, neglecting possible losses of mass from the surface. Corrosion rate was also formulated by Eq. (2) and a fitting parameter shows $K_p^{0.5} = 0.20\ \mu m\ h^{-1}$ for JPCA similar value with the averaged corrosion depth in F82H at 450 °C.

3.6. Hardness

Table 3 shows Vickers hardness (HV) of the parent material, heat affected zone and weldment region in unused and tested specimens. Hardness was represented by the range of measured values and the average in parentheses. Ten measurements were performed 2.4 mm from the surface. The weld in the untested F82H showed HV250–270 which was the largest among three positions. Parent material had an average hardness of HV212

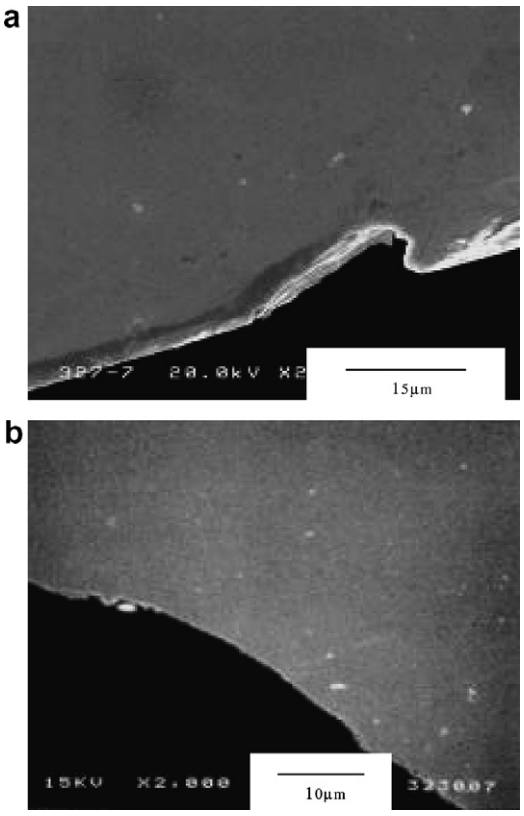

Fig. 7. Pit observed in JPCA tested at 450 °C for (a) top 1000 h and (b) bottom 3000 h at the round corners.

which was as hard as the heat affected zone. On the contrary the heat affected zone in the untested JPCA showed a hardness of HV160–180 which was the largest among three sample locations. Parent material had an average hardness of HV152, which was almost the same hardness as measured for the weld. A change of HV was not seen in both materials after corrosion test.

4. Discussion

The oxide layer of the ferritic–martensitic steels is generally composed of two zones at low temperature, ca, 470 °C [6]. In this study it is confirmed that the oxide layer in F82H also consisted of two different types of oxide layers when tested at 450 °C, and in addition an oxygen diffusion region was detected at the inner side at 500 °C. A failure of oxide layers was seen in the sample tested under the condition of 500 °C and 1000 h. The width of failed oxide layer was less than 2–3 μm as shown in Figs. 3(c) and (d). But the oxide layer formed by 3000 h at the same temperature, shown in Fig. 3(e), did not have any broken surface. The stable oxide development observed at 450 °C did not work at 500 °C. Oxide layers were damaged seriously as shown in Fig. 3(f). Separation of oxide layers from the material surface will enhance corrosion rate substantially as shown in Fig. 5. Corrosion behavior of F82H under LBE flow was previously reported to be severe erosion at 550 °C [7]. It is evaluated that F82H can be used in LBE flow below 500 °C without an added surface protecting mechanism. From the results of X-ray diffraction analyses shown in Fig. 10, the diffraction peak angles indicated a formation of $M(Fe,Cr)_3O_4$ type oxide. And from element mapping results on Fe and Cr distribution it can be concluded that the outer oxide layer is a magnetite Fe_3O_4 and the inner layer is a spinel type $FeCr_2O_4$.

The corrosion properties of an austenitic stainless steel at low temperature, below 470 °C showed good endurance for materials usage in LBE during a short time, ca, 3000 h [6,8], although a dissolution of Ni from parent materials into LBE must be considered during long time exposure [9,10]. Corrosion behavior in JPCA was characterized by oxide layers at 500 °C and pit formation at 450 °C. The X-ray diffraction peaks indicate that the oxide type corresponded to M_3O_4. A development of oxide layer is recognized by increasing the number of diffraction peaks at 450 °C. At 500 °C a significant peak corresponding to M_3O_4 was observed in 1000 h. A development of a pit is estimated to be widening the pit size but not to be deepening the hole by comparing the pit shape at 3000 h with that at 1000 h as shown in Fig. 7. Pits were only observed in the tip region where LBE impinged to the specimen in the channel. So an isothermal flow simulation was done to determine the LBE flow profile around the specimen in the channel by using STAR-CD code [11].

Fig. 14 shows the results under the conditions that the main flow velocity of LBE is 0.5 m/s, diameter of test holder is 12 mm, kinetic viscosity is 0.15 mm^2/s, and k–ε model for describing turbulence. The Reynolds number is 4×10^4 in the channel. Contour lines indicate averaged flow velocity and the arrows indicate the velocity vector. Around the specimen tip, flow is stagnant. A maximum velocity of 1.1 m/s is reached near the round corner where the velocity is accelerated rapidly. Along the side surface of specimen the main flow velocity becomes almost constant. Pits were observed on the round corners for JPCA specimen. The location corresponds to the area where LBE flow is accelerated. Pits were not formed on F82H. The difference between JPCA and F82H can be understood by the hardness and oxide layer. The reason for reduced pitting may be attributed to larger hardness in F82H than JPCA as listed in Table 3. Pits were not recognized at 500 °C though hardness is decreased but this is because the surface is damaged by corrosion.

The amount of data to describe corrosion rate in this experiment is small. Reference data on 9Cr–1Mo and 2.25Cr–1Mo steels obtained in the same loop [12] are added in Fig. 12. Corrosion rates of added data showed the same trend observed with F82H at 450 °C, described by a parabolic rule. Corrosion depth was defined by the sum of the thickness of both the oxide layer and pit depth in JPCA. Oxide layer was 1–2 μm in depth by 3000 h but the pit depth was relatively large at 450 °C. Again reference data on SS316 obtained in the same loop [12] are added in Fig. 13. For the case of the additional reference data for SS316, there was no impinging flow in the channel so that pits were not observed. The corrosion rate could be evaluated to be within 5 μm in these stainless steels.

The oxidation kinetics of the steel in the flowing LBE was proposed by the next equation [13]:

$$D = (K_p t)^{0.5} - 2/3 K_r t. \quad (3)$$

The equation means that the corrosion mechanism is explained by both an oxide scale formation and a scale removal, where D is corrosion depth, K_p is a parabolic oxide growth rate constant, K_r is a scale removal rate constant and t is time. Zhang and Li calculated K_p and K_r to be 3.21×10^{-17} m^2/s and 9.1×10^{-13} m/s, respectively, in the rate control process of forming a two-layer oxide layer in the steel at 550 °C [13]. In this study a loss of mass was ignored and a parabolic law was adopted to characterize D. K value, 2.67×10^{-17} m^2/s ($K^{0.5} = 0.31$ μm) is roughly equal to the K_p in the Eq. (3) in a short time range because the second term in the Eq. (3) is less than a several μm if $K_r = 3.21 \times 10^{-17}$ m^2/s is adopted to the F82H case. However, for a log time range evaluation of corrosion depth in flowing LBE, a mechanism of mass loss due to continuous scale removal or discrete cracking will be important. Actually, we observed cracks in the oxide layer parallel to the

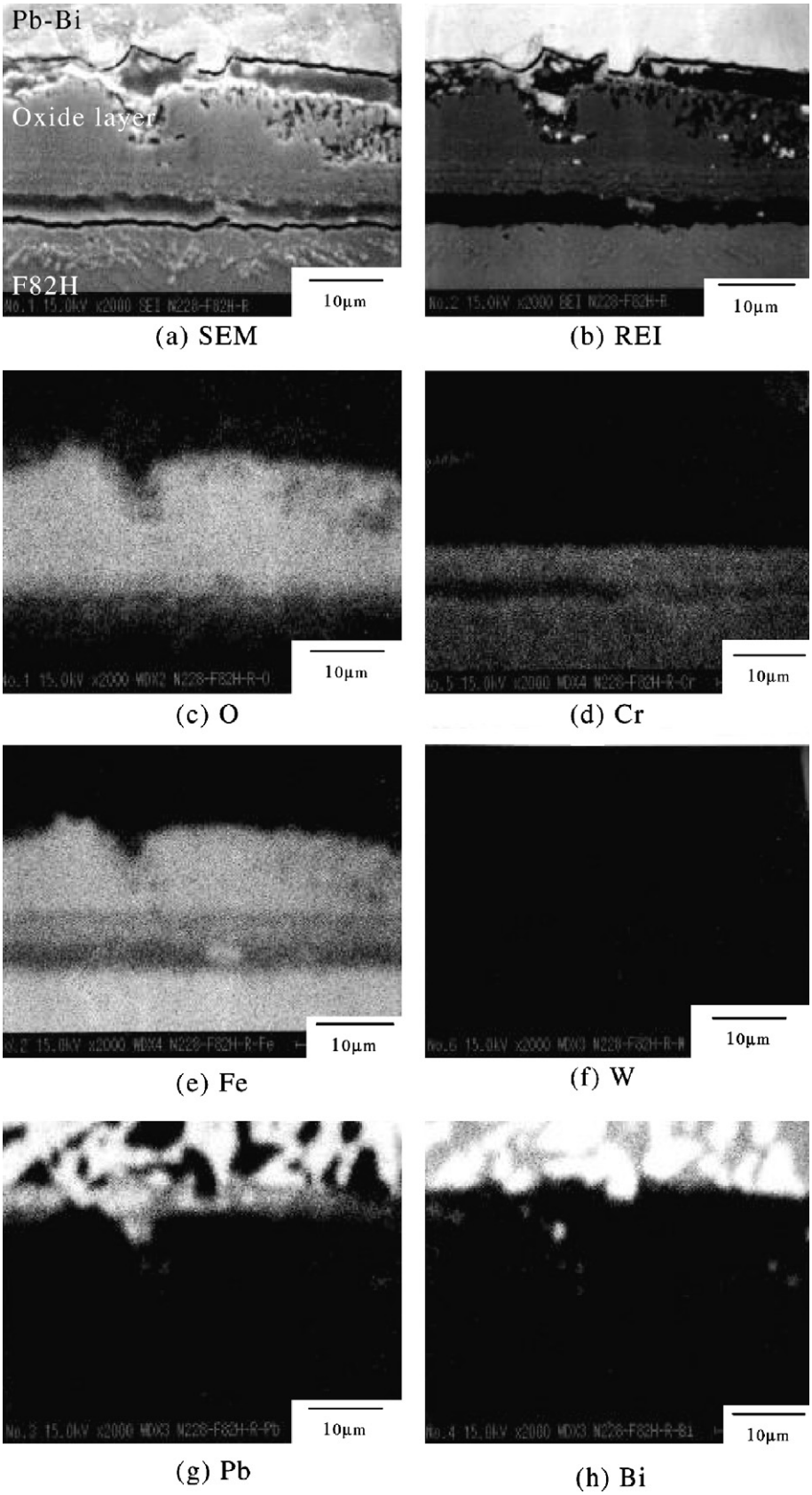

Fig. 8. EPMA results of F82H, tip, 500 °C, 1000 h.

material surface of both F82H and JPCA ay 500 °C as shown in Figs. 5 and 6. This suggests that the oxide layer grown to 10 μm/1000 h is easy to be removed. So that for long times a linear law, D [μm] = 0.01t [h] is recommended for design use, which is plotted as the solid lines in the Figs. 12 and 13. In the design of reference ADS, a proton beam window is to be replaced every year.

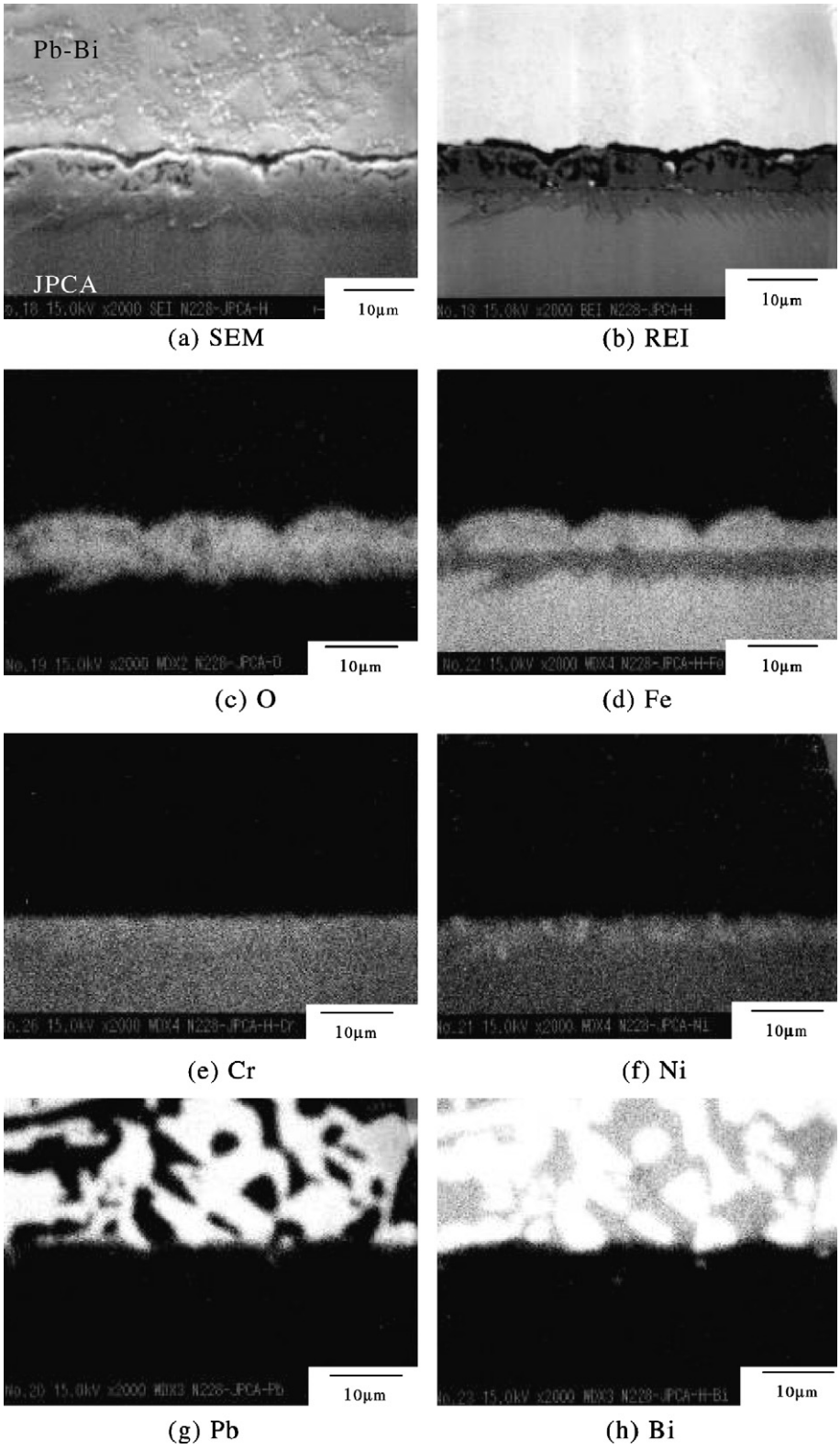

Fig. 9. EPMA results of JPCA near welded region, 500 °C, 1000 h.

5. Conclusions

Corrosion behavior of a ferritic–martensitic steel F82H, and austenitic stainless steel JPCA was studied in an LBE loop under active oxygen control to $2–4 \times 10^{-5}$ mass%. The following conclusions were obtained.

The corrosion layer of F82H consists of three structures; that is, the outer oxide layer is a magnetite Fe_3O_4, the inner layers are a spinel type $FeCr_2O_4$ and an oxygen diffusion layer. Corrosion depth increased with increasing time at 450 °C, and with increasing test temperature. The oxide layer was repaired by the newly formed oxide at 450 °C. Early corrosion rate followed a parabolic rule.

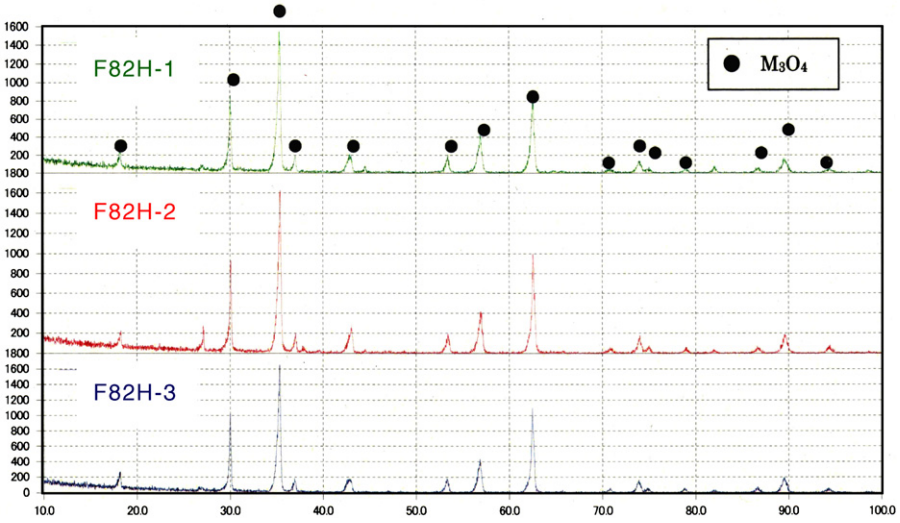

Fig. 10. X-ray diffraction analyses of F82H specimens under the condition of 1000 h at 450 °C (top), 1000 h at 500 °C (middle) and 3000 h at 450 °C (bottom).

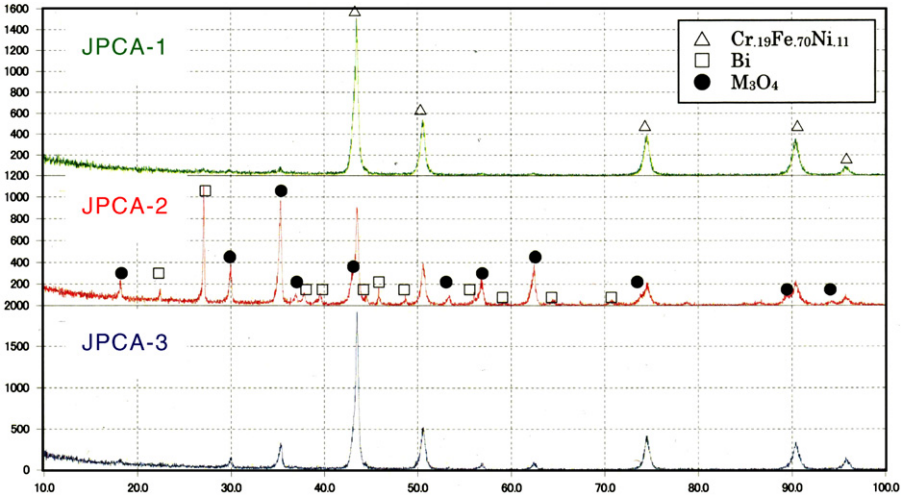

Fig. 11. X-ray diffraction analyses of JPCA specimens under the condition of 1000 h at 450 °C (top), 1000 h at 500 °C (middle) and 3000 h at 450 °C (bottom).

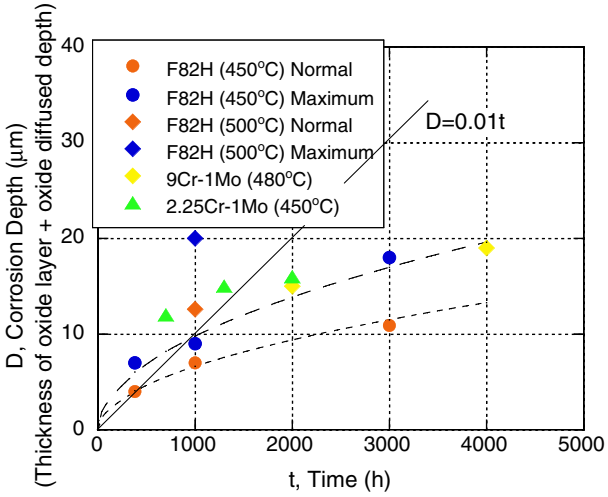

Fig. 12. Corrosion rate, μm h^{-1}, of F82H.

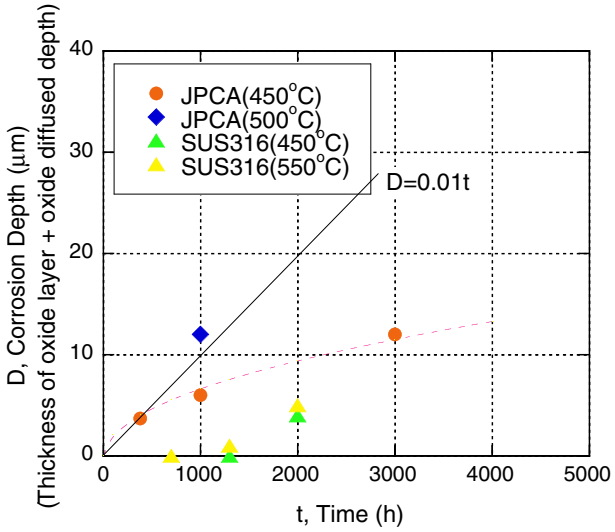

Fig. 13. Corrosion rate, μm h^{-1}, of JPCA.

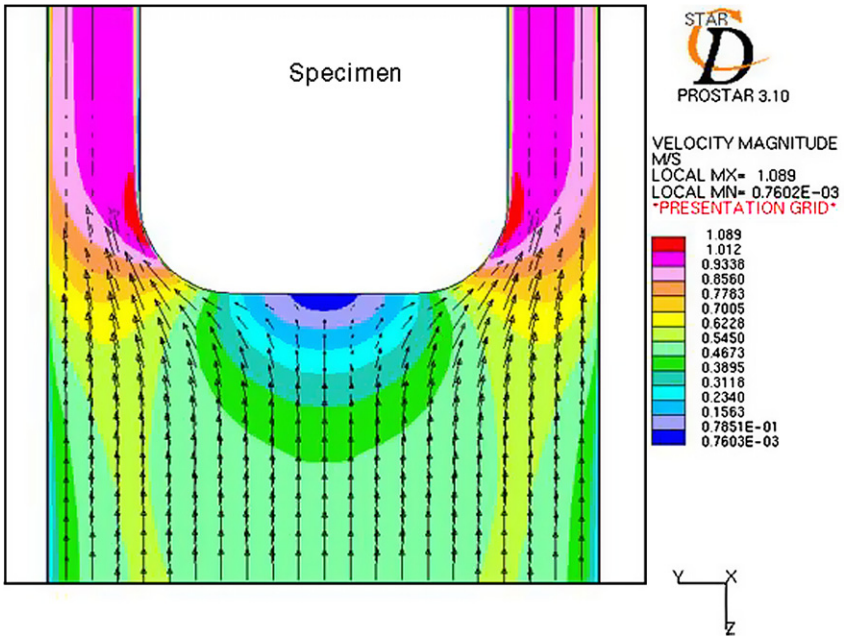

Fig. 14. Flow simulation of liquid Pb–Bi around specimen in the test holder.

Table 3
Hardness (100gf)

Specimens		Parent material	HAZ	Weldment
F82H	Before	207–218(214)	202–219(210)	257–274(267)
	After	203–218(210)	179–213(204)	250–269(262)
JPCA	Before	144–159(152)	160–181(173)	153–165(159)
	After	141–159(154)	158–183(172)	148–174(161)

The ranges of measured values are shown.
The averaged values are in the parenthesis.

The corrosion layer at 500 °C in F82H disintegrated during testing. EB welded joint showed the same corrosion properties as the parent materials.

The corrosion behavior in JPCA was characterized by the oxide layer Fe_3O_4 and pit formation. At 450 °C, the oxide layer was 1–2 μm in depth by 3000 h but pit depth was relatively large. EB welded joint showed the same corrosion property as the parent materials.

Corrosion rates were characterized by a parabolic law within the test time range for both materials including weld joints at 450 °C and 500 °C. Oxide layers of both materials at 500 °C were disintegrated and unstable by cracking in the oxide layer parallel to the material surface. So that corrosion depth D [μm] = $0.01t$ [h] is recommended to use in the ADS beam design.

Acknowledgement

This work was partly entrusted by the Ministry of Education, Culture, Science and Sports Technology (MEXT).

References

[1] K. Kikuchi, T. Sasa, S. Ishikura, K. Mukugi, T. Kai, N. Ouchi, I. Ioka, J. Nucl. Mater. 296 (2001) 34.
[2] M. Tamura, H. Hayakawa, M. Tanimura, A. Hishinuma, T. Kondo, J. Nucl. Mater. 141–143 (1986) 620.
[3] M.P. Tanaka, P.J. Maziasz, A. Hishinuma, S. Hamada, J. Nucl. Mater. 141–143 (1986) 943.
[4] K.Tsujimoto, T.Sasa, K.Nishihara, T Takizuka, H. Takano, Study of Accelerator-driven System for Transmutation of High-level Waste from LWR, ICONE-7, Tokyo, 1999.
[5] M.Ono, T. Mine, K.Kamata, T. Kitano, MES Lead Bismuth Forced Circulation Loop and Test Results ICONE-11, Tokyo, 2003.
[6] F. Barbier, A. Rusanov, J. Nucl. Mater. 296 (2001) 231.
[7] M. Kondo, M. Takahashi, T. Suzuki, K. Ichikawa, K. Hata, S. Qiu, H. Sekimoto, J. Nucl. Mater. 343 (2005) 349.
[8] G. Muler, A. Heinzel, J. Koney, G. Schumacher, A. Weisenburger, F. Zimmermann, V. Engelko, A. Rusanov, V. Markov, J. Nucl. Mater. 301 (2002) 40.
[9] O. Martinov, Y. Orlov, A. Efanov, V. Troinov, A. Rusanov, O. Lavrova, in: Proceedings of ISTC-RITech Japan Workshop on Nuclear Reactor Technologies in Russia/CIS, vol. 9, 2001, p. 80.
[10] K. Kikuchi, S. Saito, Y. Kurata, M. Futakawa, T. Sasa, H. Oigawa, E. Wakai, M. Umeno, H. Mizubayashi, K. Miura, JSME Int. J. B 47 (2) (2004) 332–339.
[11] Star-CD User Guide, CD Adaco Japan Co., Ltd., 2002.
[12] K. Kamata, private communication.
[13] J. Zhang, N. Li, Oxid. Met. 63 (516) (2005) 353.
[14] F. Barbier, A. Rusanov, J. Nucl. Mater. 296 (2001) 231.
[15] D.G. Briceno, F.J.M. Munoz, L.S. Crespo, F. Esteban, C. Torres, J. Nucl. Mater. 296 (2001) 265.
[16] C. Fazio, I. Ricapito, G. Scaddozzo, G. Benamati, J. Nucl. Mater. 318 (2003) 325.
[17] K. Kikuchi, Y. kurata, S. Saito, M. Futakawa, T. Sasa, H. Oigawa, E. Wakai, K. Miura, J. Nucl. Mater. 318 (2003) 348.
[18] M. Kondo, M. Takahashi, T. Suzuki, K. Ishikawa, K. Hata, S. Qiu, H. Sekimoto, J. Nucl. Mater. 348 (2005) 343.
[19] B.F. Gromov, Y.I. Orlov, P.N. Martynov, V.A. Gulevsky, Proceedings of HLMC, 1999, p. 87.